Four-electron oxidation of *p*-hydroxylaminobenzoate to *p*-nitrobenzoate by a peroxodiferric complex in AurF from *Streptomyces thioluteus*

Ning Li[a,1], Victoria Korneeva Korboukh[a,b,1], Carsten Krebs[a,b,2], and J. Martin Bollinger, Jr.[a,b,2]

[a]Departments of Biochemistry and Molecular Biology and [b]Chemistry, Pennsylvania State University, University Park, PA 16802

Edited by Harry B. Gray, California Institute of Technology, Pasadena, CA, and approved July 16, 2010 (received for review March 3, 2010)

The nonheme di-iron oxygenase, AurF, converts *p*-aminobenzoate (Ar-NH_2, where Ar = 4-carboxyphenyl) to *p*-nitrobenzoate (Ar-NO_2) in the biosynthesis of the antibiotic, aureothin, by *Streptomyces thioluteus*. It has been reported that this net six-electron oxidation proceeds in three consecutive, two-electron steps, through *p*-hydroxylaminobenzoate (Ar-NHOH) and *p*-nitrosobenzoate (Ar-NO) intermediates, with each step requiring one equivalent of O_2 and two exogenous reducing equivalents. We recently demonstrated that a peroxodiiron(III/III) complex (peroxo-$Fe_2^{III/III}$-AurF) formed by addition of O_2 to the diiron(II/II) enzyme ($Fe_2^{II/II}$-AurF) effects the initial oxidation of Ar-NH_2, generating a μ-(oxo)diiron (III/III) form of the enzyme (μ-oxo-$Fe_2^{III/III}$-AurF) and (presumably) Ar-NHOH. Here we show that peroxo-$Fe_2^{III/III}$-AurF also oxidizes Ar-NHOH. Unexpectedly, this reaction proceeds through to the Ar-NO_2 final product, a four-electron oxidation, and produces $Fe_2^{II/II}$-AurF, with which O_2 can combine to regenerate peroxo-$Fe_2^{III/III}$-AurF. Thus, conversion of Ar-NHOH to Ar-NO_2 requires only a single equivalent of O_2 and (starting from $Fe_2^{II/II}$-AurF or peroxo-$Fe_2^{III/III}$-AurF) is fully catalytic in the absence of exogenous reducing equivalents, by contrast to the published stoichiometry. This novel type of four-electron *N*-oxidation is likely also to occur in the reaction sequences of nitro-installing di-iron amine oxygenases in the biosyntheses of other natural products.

aureothin | di-iron | N-oxygenase | nonheme | nitroarene

The enzyme AurF from *Streptomyces thioluteus* converts *para*-aminobenzoate (Ar-NH_2, where Ar = 4-carboxyphenyl) to *para*-nitrobenzoate (Ar-NO_2) in the biosynthesis of the antibiotic, aureothin (1, 2). It is structurally similar to the β_2 subunits of class I ribonucleotide reductases and the oxygenase components of bacterial multicomponent monooxygenases (BMMs), which all use carboxylate-bridged di-iron clusters to activate O_2 (3–5). Following some initial controversy over whether the active form of AurF also contains a di-iron cluster (6) or, instead, a dimanganese (7, 8) or manganese/iron cluster (9), two recent studies established unequivocally that the di-iron form is active (although they did not rule out the possibility that the manganese/iron form could also be active) (10, 11). The first study showed that Fe_2-AurF could convert Ar-NH_2 to Ar-NO_2 in the presence of O_2 and a reducing system (although not the native reductase, which has not yet been identified) (10). It reasserted the previously proposed reaction sequence comprising three canonical diiron-oxygenase cycles (6), each involving, first, combination of O_2 with the diiron(II/II) form of the enzyme ($Fe_2^{II/II}$-AurF) to form an intermediate that oxidizes the substrate (Ar-NH_2, Ar-NHOH, and Ar-NO in cycles one, two, and three, respectively) by two electrons and, second, reduction of the resultant diiron(III/III) form of the enzyme ($Fe_2^{III/III}$-AurF) back to the O_2-reactive $Fe_2^{II/II}$-AurF (Scheme 1*A*). It purported to detect the Ar-NO intermediate of the second cycle [Ar-NHOH having already been detected previously (6, 7)] and discussed the nature of its formation (10). Whereas the Hertweck group proposed hydroxylation of Ar-NHOH to Ar-$N(OH)_2$ followed by dehydration

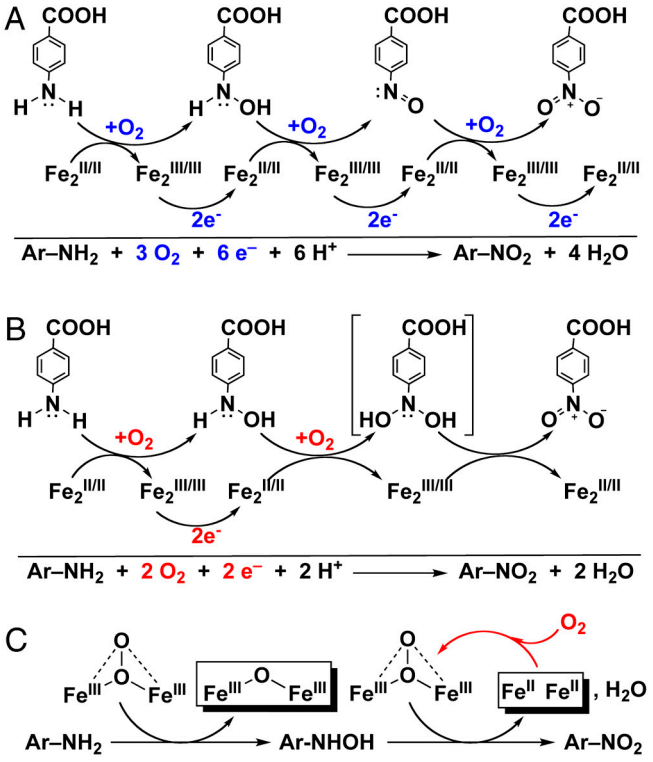

Scheme 1. Reactions catalyzed by AurF. (*A*) Previously proposed stoichiometry of the AurF-catalyzed conversion of Ar-NH_2 to Ar-NO_2 (8–10); (*B*) stoichiometry of the AurF-catalyzed reaction indicated by this study; and (*C*) reactions of peroxo-$Fe_2^{III/III}$-AurF with Ar-NH_2 and Ar-NHOH.

to Ar-NO (7, 8), Zhao and coworkers reasserted their previous proposal that Ar-NHOH undergoes direct dehydrogenation to Ar-NO (10). The basis for this proposal was isotopic labeling studies, which had shown that reaction of Ar-$NH^{16}OH$ in the presence of $^{18}O_2$(g) results in incorporation of only one atom of ^{18}O into the Ar-NO_2 (6). This labeling pattern is consistent with the formation of the presumptive Ar-$N^{16}O$ intermediate by a dehydrogenation mechanism, which would leave it devoid of any ^{18}O label, so that the third oxidation step with $^{18}O_2$ would then gen-

Author contributions: N.L., V.K.K., C.K., and J.M.B. designed research; N.L. and V.K.K. performed research; N.L. and V.K.K. contributed new reagents/analytic tools; N.L., V.K.K., C.K., and J.M.B. analyzed data; and N.L., C.K., and J.M.B. wrote the paper.

The authors declare no conflict of interest.

This article is a PNAS Direct Submission.

Freely available online through the PNAS open access option.

[1]N.L. and V.K.K. contributed equally to this work.

[2]To whom correspondence may be addressed. E-mail: jmb21@psu.edu or ckrebs@psu.edu.

This article contains supporting information online at www.pnas.org/lookup/suppl/doi:10.1073/pnas.1002785107/-/DCSupplemental.

erate Ar-N(^{16}O)(^{18}O) with only one atom of ^{18}O (Scheme S1, Zhao pathway). The labeling pattern is inconsistent with formation of Ar-NO by hydroxylation to Ar-N(^{16}OH)(^{18}OH) followed by dehydration, which should result in a 1:1 mixture of Ar-N^{16}O and Ar-N^{18}O (assuming no isotope effect nor stereochemical bias in the dehydration step) and, in the absence of exchange with solvent of the O-atom from the nitroso group, subsequently result in formation of a 1:1 mixture of Ar-N(^{16}O)(^{18}O) and Ar-N(^{18}O)$_2$ in the final oxidation step (Hertweck pathway).

The second study to confirm the activity of Fe_2-AurF reported trapping and characterization of a long-lived peroxodiiron(III/III) complex (peroxo-$Fe_2^{III/III}$-AurF) that is competent to oxidize Ar-NH_2 (presumably to Ar-NHOH, but this intermediate was not explicitly verified) (11). The nearly complete conversion of Ar-NH_2 to the fully oxidized Ar-NO_2 at low ratios of Ar-NH_2/peroxo-$Fe_2^{III/III}$-AurF (<0.3) suggested that the peroxide complex might also be capable of the two subsequent oxidations (Ar-NHOH → Ar-NO → Ar-NO_2). In this study, we have confirmed that the two-electron-oxidized substrate species (Ar-NHOH) does indeed react with peroxo-$Fe_2^{III/III}$-AurF. The reaction does not, however, generate Ar-NO and a diiron(III/III) cluster, the products expected from the published reaction sequence (7, 9, 10) and our previous study (11). Rather, the reaction generates $Fe_2^{II/II}$-AurF and the fully oxidized Ar-NO_2, implying that a four-electron redox process occurs. In the presence of excess O_2, the $Fe_2^{II/II}$-AurF so produced regenerates peroxo-$Fe_2^{III/III}$-AurF, priming for oxidation of another molecule of Ar-NHOH. Thus, the reaction is catalytic without exogenous reducing equivalents. The results mandate reformulation of the overall conversion of Ar-NH_2 to Ar-NO_2 by Fe_2-AurF (Scheme 1*B*) and reevaluation of the mechanism of the last two oxidation steps. Specifically, they suggest that the Ar-NH_2 → Ar-NO_2 conversion proceeds by a sequence of two consecutive, mechanistically analogous hydroxylations followed by an inner-sphere, proton-coupled, two-electron transfer (Scheme 1*B*), rather than by the alternating, mechanistically distinct hydroxylation, dehydrogenation, and hydroxylation steps previously proposed (Scheme 1*A*). The new mechanism, which accounts simply for the aforementioned $^{18}O_2$ isotope labeling experiments (Scheme S1, central pathway), invokes a four-electron *N*-oxidation, which is initiated by a peroxodiiron (III/III) intermediate and is, to the best of our knowledge, unprecedented.

Results

Testing for a Reaction Between Peroxo-$Fe_2^{III/III}$-AurF and Ar-NHOH by Stopped-Flow Absorption (SF-Abs) Experiments. Our recent study showed that mixing $Fe_2^{II/II}$-AurF with O_2 results in rapid formation of peroxo-$Fe_2^{III/III}$-AurF, which can be monitored by its absorption at 500 nm with molar absorptivity of ~500 M^{-1} cm^{-1} (11). Subsequent mixing of the intermediate with Ar-NH_2 results in a rapid decrease in absorbance at this wavelength (A_{500}), reflecting oxidation of Ar-NH_2 by peroxo-$Fe_2^{III/III}$-AurF. A_{500}-versus-time traces from similar, sequential-mixing, SF-Abs experiments, in which peroxo-$Fe_2^{III/III}$-AurF was formed by an initial mix of $Fe_2^{II/II}$-AurF with O_2 and then exposed to Ar-NHOH in the second mix, show that the two-electron-oxidized substrate species also reacts efficiently (Fig. 1). Revealingly, the kinetic behavior depends markedly on the relative concentrations of AurF, O_2, and Ar-NHOH. When the initial mix to form peroxo-$Fe_2^{III/III}$-AurF delivers ~2 equiv O_2 and the second mix delivers 1 equiv Ar-NHOH, A_{500} decreases rapidly, reaches a minimum after ~50 ms, and then increases to approximately the original value (red traces in Fig. 1 *A* and *B*). By contrast to this transient behavior, A_{500} decreases and remains stable when ~2 equiv O_2 is delivered in the first mix and ≥2 equiv Ar-NHOH is delivered in the second mix (Fig. 1*A*, blue and green traces). Similarly, A_{500} decreases and remains stable if ≤1 equiv O_2 is delivered in the first mix and ≥1 equiv Ar-NHOH is delivered in the second mix (Fig. 1*B*, blue trace). These observations can all be explained by assuming that the reaction between Ar-NHOH and peroxo-$Fe_2^{III/III}$-AurF generates $Fe_2^{II/II}$-AurF. With overall O_2/Ar-NHOH/AurF ratios of 2/1/1, one equiv O_2 remains after the first has been used to form peroxo-$Fe_2^{III/III}$-AurF. This remaining O_2 adds to the $Fe_2^{II/II}$-AurF produced by reaction of the first equiv of peroxo-$Fe_2^{III/III}$-AurF with Ar-NHOH, generating a second equiv of peroxo-$Fe_2^{III/III}$-AurF and yielding the transient kinetic behavior. With O_2/Ar-NHOH/AurF = 2/ ≥ 2/1, sufficient substrate remains to consume the second equiv of peroxo-$Fe_2^{III/III}$-AurF, O_2 is at that point exhausted, and the $Fe_2^{II/II}$-AurF is then stable. With O_2/Ar-NHOH/AurF = 1/1/1, O_2 is exhausted in the initial formation of peroxo-$Fe_2^{III/III}$-AurF, and the $Fe_2^{II/II}$-AurF generated upon reaction with Ar-NHOH is again stable.

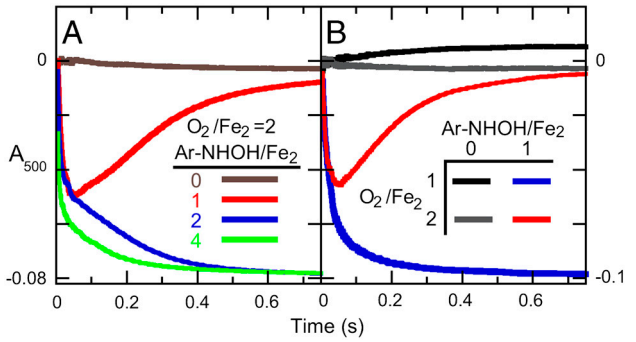

Fig. 1. Sequential-mixing SF-Abs experiments to monitor the reaction of peroxo-$Fe_2^{III/III}$-AurF with Ar-NHOH. (*A*) A solution of $Fe_2^{II/II}$-AurF (0.9 mM Fe_2) was mixed with an equal volume of reaction buffer (see *Experimental Procedures* for composition) containing 1.8 mM O_2 ($O_2/Fe_2 = 2$). This solution was allowed to react at 5 °C for 0.5 s to permit accumulation of peroxo-$Fe_2^{III/III}$-AurF and was then mixed with an equal volume of an O_2-free solution of Ar-NHOH (in buffer) at concentrations appropriate to give the Ar-NHOH/Fe_2 ratios indicated in the inset. (*B*) A solution of $Fe_2^{II/II}$-AurF (0.9 mM Fe_2) was mixed with an equal volume of reaction buffer containing either 0.9 mM (black and blue) or 1.8 mM O_2 (gray and red). This solution was allowed to react at 5 °C for 0.5 s to permit accumulation of peroxo-$Fe_2^{III/III}$-AurF and was then mixed with an equal volume of an O_2-free solution of buffer (black and gray) or 0.45 mM Ar-NHOH (blue and red).

Evaluation of Di-iron Products in Reaction of Peroxo-$Fe_2^{III/III}$-AurF with Ar-NHOH by Mössbauer Spectroscopy. Mössbauer spectroscopic experiments were conducted to test the conclusion that reaction of peroxo-$Fe_2^{III/III}$-AurF with Ar-NHOH produces $Fe_2^{II/II}$-AurF, which is stable when O_2 is limiting and transient when O_2 is in excess. The 4.2-K/53-mT spectrum of a sample prepared by reacting $Fe_2^{II/II}$-AurF with limiting (0.75 equiv) O_2 reveals that peroxo-$Fe_2^{III/III}$-AurF is the predominant species in the sample (vertical bars in Fig. 2*A*). The red line plotted over the data is a "reference spectrum" of the intermediate complex, which was generated by analysis of the experimental spectrum of a sample that was prepared so as to yield a maximum fraction of the intermediate (see Fig. S1 for the reaction conditions, explanation of the analysis, and the Mössbauer parameters). The reference spectrum accounts for 62% of the total intensity of the experimental spectrum in Fig. 2*A*. (We estimate an uncertainty of ±3 on this and all other percentages of total absorption area given in the text.) As expected, use of limiting O_2 results in a significant fraction (36%) of unreacted $Fe_2^{II/II}$-AurF starting material (δ = 1.23 mm/s, ΔE_Q = 3.08 mm/s; blue line). A minor fraction (6%) of μ-oxo-$Fe_2^{III/III}$-AurF is also present (δ = 0.54 mm/s, ΔE_Q = 1.86 mm/s, green line). Treatment of an identical sample with one equiv Ar-NHOH for 45 ms or 400 ms prior to rapid freezing (freeze-quenching) results in marked spectral changes (vertical bars in Fig. 2 *B* and *C*, respectively, and Fig. S2). The features of peroxo-$Fe_2^{III/III}$-AurF decay (to 33% and 8%, respec-

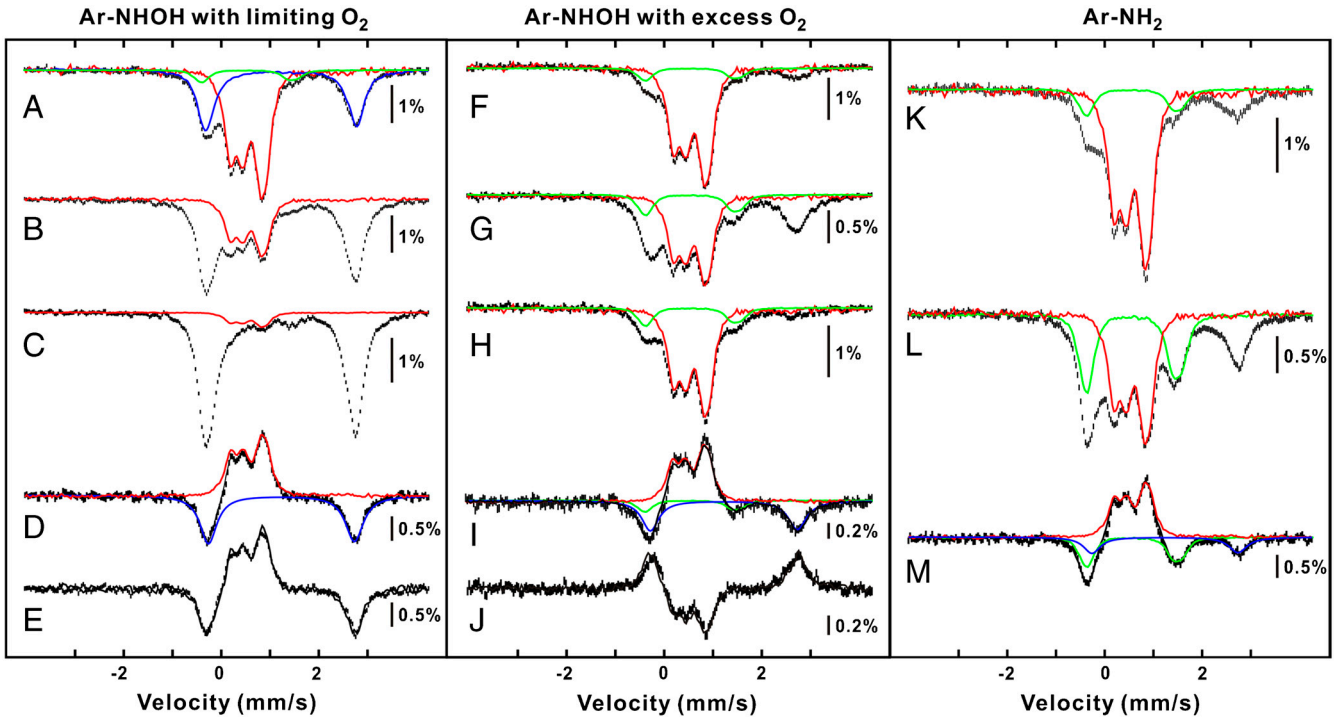

Fig. 2. 4.2-K/53-mT Mössbauer spectra of samples in which peroxo-$Fe_2^{III/III}$-AurF was reacted with Ar-NHOH or Ar-NH_2. In all cases, the red, blue, and green lines illustrate the fractional contributions of the reference spectra of peroxo-$Fe_2^{III/III}$-AurF, $Fe_2^{II/II}$-AurF, and μ-oxo-$Fe_2^{III/III}$-AurF, respectively, to the experimental spectrum, as described in the text. (*Left*) A solution of $Fe_2^{II/II}$-AurF (1.2 mM Fe_2) was mixed with 0.5 equivalent volume of buffer solution containing 1.8 mM O_2 ($O_2/Fe_2 = 0.75$). This solution was allowed to react at 5 °C for 0.11 s to permit accumulation of peroxo-$Fe_2^{III/III}$-AurF. (*A*) The solution was then directly freeze-quenched. (*B* and *C*) The solution was then mixed with one-sixth equivalent volume of an O_2-free solution of 3.6 mM Ar-NHOH (Ar-NHOH/$O_2 = 1$), and this solution was allowed to react for 45 ms (*B*) or 400 ms (*C*) prior to being freeze-quenched. *D* and *E* are the difference spectra *B-A* and *C-B*, respectively. The black line in *D* is the sum of the contributions of peroxo-$Fe_2^{III/III}$-AurF (−28%) and $Fe_2^{II/II}$-AurF (28%). The black line in *E* is the difference spectrum *B-A* for comparison. (*Middle*) A solution of $Fe_2^{II/II}$-AurF (1.8 mM) was mixed with two equivalent volumes of a buffer solution containing 1.8 O_2 mM O_2 ($O_2/Fe_2 = 2$). This solution was allowed to react at 5 °C for 110 ms to permit accumulation of peroxo-$Fe_2^{III/III}$-AurF. (*F*) The reaction was then directly freeze-quenched. (*G* and *H*) The solution was then mixed with one-sixth equivalent volume of an O_2-free buffer solution containing 3.6 mM Ar-NHOH (Ar-NHOH/$O_2 = 0.5$), and this reaction was allowed to proceed at 5 °C for 45 ms (*G*) or 2 s (*H*) prior to being freeze-quenched. *I* and *J* are the difference spectra *G-F* and *H-G*, respectively. The black line in *J* is difference spectrum *C–B*, scaled by a factor of −0.8 for comparison. (*Right*) A solution of $Fe_2^{II/II}$-AurF (1.2 mM) was mixed with 0.5 equivalent volume of a buffer solution containing 1.8 mM O_2 ($O_2/Fe_2 = 0.75$), and the reaction was allowed to proceed at 5 °C for 110 ms to permit accumulation of peroxo-$Fe_2^{III/III}$-AurF. (*K*) The reaction was directly freeze-quenched. (*L*) The resulting solution was then mixed with one-sixth equivalent volume of an O_2-free buffer solution containing 0.91 mM Ar-NH_2 (Ar-$NH_2/O_2 = 0.25$), and the reaction was allowed to proceed for 4 s before being freeze-quenched. *M* is the difference spectrum *L–K*. The black line in *M* is the sum of the contributions of peroxo-$Fe_2^{III/III}$-AurF (−29%), $Fe_2^{II/II}$-AurF (12%), and μ-oxo-$Fe_2^{III/III}$-AurF (17%).

tively; red lines), and features attributable to $Fe_2^{II/II}$-AurF grow in. The contribution from μ-oxo-$Fe_2^{III/III}$-AurF remains constant. The changes are best illustrated by the difference spectrum generated by subtracting 2*A* from 2*B* (Fig. 2*D*, vertical bars). In this presentation, the features pointing upward are associated with the decaying species (peroxo-$Fe_2^{III/III}$-AurF; red line), and the features pointing downward with the developing species ($Fe_2^{II/II}$-AurF; $\delta = 1.23$ mm/s, $\Delta E_Q = 3.00$ mm/s; blue line). We note that the measured quadrupole splitting parameter, ΔE_Q, of the developing Fe^{II} species (3.00 mm/s) is slightly different from that of the reactant $Fe_2^{II/II}$-AurF complex ($\Delta E_Q = 3.08$ mm/s), suggesting that cycling through the peroxo-$Fe_2^{III/III}$-AurF state might cause a conformational change at the $Fe_2^{II/II}$ cluster, as was observed for the diiron-carboxylate oxidase, stearoyl-acyl carrier protein Δ^9 desaturase (12). The summation of the appropriately weighted reference spectra for the decaying peroxo-$Fe_2^{III/III}$-AurF (−28%) and the developing $Fe_2^{II/II}$-AurF (28%) agrees well with the experimental difference spectrum (compare solid black line and vertical bars in Fig. 2*D*). The difference between the spectra of the 400-ms and 45-ms samples (*C-B*, Fig. 2*E* vertical bars) is, within the experimental uncertainty, identical to the *B-A* difference spectrum (Fig. 2*E*, solid line) and again demonstrates conversion of 28% of peroxo-$Fe_2^{III/III}$-AurF to 28% of $Fe_2^{II/II}$-AurF. The similarity of these two difference spectra strongly suggests that the process being monitored has only one kinetically significant step (two states, reactants and products), because a sequence of two or more steps (three or more states) ought not to give a constant difference spectrum from 0 to 45 ms and 45 ms to 400 ms. The kinetics of the conversion of peroxo-$Fe_2^{III/III}$-AurF to $Fe_2^{II/II}$-AurF reflected in the Mössbauer data are reasonably consistent with those determined by SF-Abs. One minor inconsistency is that 8% of peroxo-$Fe_2^{III/III}$-AurF remains at 400 ms, whereas the SF-Abs data indicate that decay should be essentially complete by this reaction time (Fig. 1*B*, blue trace). We attribute this remaining peroxo-$Fe_2^{III/III}$-AurF to the reaction of a small fraction of the $Fe_2^{II/II}$-AurF product with O_2 from the air during passage through the freeze-quench reaction hose and into the cryosolvent.

The 4.2-K/53-mT Mössbauer spectrum of a sample prepared by reacting $Fe_2^{II/II}$-AurF with ∼2 equiv O_2 per diiron cluster (Fig. 2*F*, vertical bars) indicates the presence of 82% peroxo-$Fe_2^{III/III}$-AurF (red line) and 9% each of μ-oxo-$Fe_2^{III/III}$-AurF and $Fe_2^{II/II}$-AurF. The spectra of identical samples that were subsequently mixed with one equiv Ar-NHOH and then allowed to react for 45 ms (Fig. 2*G*) or 2 s (Fig. 2*H*) before being freeze-quenched (see Fig. S3 for additional spectra corresponding to different reaction times) confirm the conclusion from the SF-Abs experiments that peroxo-$Fe_2^{III/III}$-AurF initially decays (to 52%

in Fig. 2*G*, red line) and is subsequently regenerated (74% in Fig. 2*H*, red line). The *G*-*F* difference spectrum (Fig. 2*I*, vertical bars) reveals the conversion of 28% of peroxo-$Fe_2^{III/III}$-AurF (red line) to 20% $Fe_2^{II/II}$-AurF (blue line) and 6% μ-oxo-$Fe_2^{III/III}$-AurF (green line). The μ-oxo-$Fe_2^{III/III}$-AurF could result from the reaction of some of the peroxo-$Fe_2^{III/III}$-AurF with small amounts of either Ar-NH_2 or Ar-NO present in the Ar-NHOH substrate solution (see Fig. S4). The *H*-*G* difference spectrum (Fig. 2*J*, vertical bars) reveals clean conversion of 20% $Fe_2^{II/II}$-AurF (blue line) to 20% peroxo-$Fe_2^{III/III}$-AurF (red line; note that the reformation of peroxo-$Fe_2^{III/III}$-AurF is reflected by inversion of the peaks). This difference spectrum is very similar to the difference spectrum 2*E* from the limiting-O_2 reaction (solid line in Fig. 2*J*, scaled by −0.8). Recovery of the peroxo-$Fe_2^{III/III}$-AurF is nearly complete (73% of total Fe, 89% of the peroxo-$Fe_2^{III/III}$-AurF initially present). This observation, together with the Mössbauer and SF-Abs data on the reaction with limiting O_2, confirm that Ar-NHOH effects a four-electron reduction of peroxo-$Fe_2^{III/III}$-AurF to $Fe_2^{II/II}$-AurF, presumably with concomitant four-electron oxidation of Ar-NHOH to Ar-NO_2 (confirmed below).

Verification of Catalytic Oxidation of Ar-NHOH by $Fe_2^{II/II}$-AurF. Our reformulation of the AurF six-electron-oxidation sequence eliminates the previously proposed requirement for a total of four exogenous electrons in the last two steps (compare Scheme 1 *A* and *B*). $Fe_2^{II/II}$-AurF should, therefore, be capable of multiple turnovers when oxidizing Ar-NHOH (Scheme 1*C*, right side). To verify this prediction, 15 μM $Fe_2^{II/II}$-AurF was incubated with 450 μM Ar-NHOH (Ar-NHOH/Fe_2 = 30) and ∼0.9 mM O_2 (O_2/Ar-NHOH ∼ 2). After 20 min at 0 °C, the small-molecule components were separated from the protein (by passage through a molecular weight filter, requiring an additional 10 min at 4 °C) and were analyzed by reverse-phase high-performance liquid chromatography (RP-HPLC; see *Experimental Procedures* and *SI Text* for details). The chromatogram of a standard solution containing 400 μM each of Ar-NH_2, Ar-NHOH, and Ar-NO_2 (Fig. 3, red trace) shows that the compounds are efficiently separated by this procedure. Injections of the individual compounds allowed the elution peaks to be assigned as indicated by the chemical structures. (Note that, because of differences in their molar absorptivities, the peak height and area for the Ar-NO_2 product is less than that for an equivalent quantity of Ar-NHOH

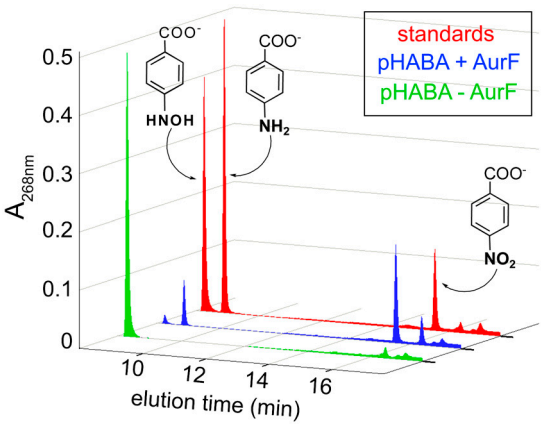

Fig. 3. Reversed-phase high-performance liquid chromatography (RP-HPLC) of the small-molecule reactants and products following incubation of $Fe_2^{II/II}$-AurF with excess Ar-NHOH and O_2. $Fe_2^{II/II}$-AurF (15 μM) was incubated with 450 μM Ar-NHOH and ∼0.9 mM O_2 for 20 min at 0 °C. Small molecules were separated from the enzyme and analyzed as described in *SI Text* (blue). A control experiment was carried out under identical conditions, except for omission of $Fe_2^{II/II}$-AurF (green). A solution containing 400 μM each of Ar-NH_2, Ar-NHOH, and Ar-NO_2 was also analyzed (red).

substrate.) The chromatogram from a control sample in which 450 μM Ar-NHOH was exposed to O_2 under the conditions of the enzyme reaction but in the absence of $Fe_2^{II/II}$-AurF (green trace) shows the prominent peak of the synthetic compound and two small peaks from unknown contaminants or decay products. This control confirms that Ar-NHOH is relatively stable on this time scale in the absence of the enzyme. The chromatogram of the experimental sample containing the enzyme (blue trace) shows that >95% (>430 μM) of the Ar-NHOH has been consumed and ∼450 μM Ar-NO_2 has been produced (estimated by comparison of the peak area to that in the chromatogram of the standard mixture). Thus, the enzyme has accomplished 28–30 turnovers in the absence of any obvious source of reducing equivalents. Catalytic oxidation of Ar-NHOH under these conditions is inconsistent with the previous formulation of the Ar-NHOH → Ar-NO → Ar-NO_2 oxidation steps (Scheme 1*A*) but entirely consistent with our reformulation (Scheme 1 *B* and *C*).

Testing for Reduction of μ-oxo-$Fe_2^{III/III}$-AurF by Ar-NHOH. The surprising ability of Ar-NHOH to reduce peroxo-$Fe_2^{III/III}$-AurF by four electrons to $Fe_2^{II/II}$-AurF and the known ability of hydroxylamine compounds to reduce Fe^{III} complexes suggested the possibility that Ar-NHOH might also reduce μ-oxo-$Fe_2^{III/III}$-AurF to $Fe_2^{II/II}$-AurF, thereby possibly permitting the six-electron-oxidation sequence to proceed without net input of *any* exogenous electrons and with only a single equivalent of O_2. However, prolonged incubation (10 min at 22 °C) of as-isolated μ-oxo-$Fe_2^{III/III}$-AurF with one equiv (1.1 mM) Ar-NHOH yielded less than 10% reduction to $Fe_2^{II/II}$-AurF (Fig. S5), implying that two exogenous electrons and two equiv O_2 are indeed required for the complete six-electron oxidation sequence.

Reevalution of the Diiron Products from the Reaction of peroxo-$Fe_2^{III/III}$-AurF with Limiting Ar-NH_2. Scheme 1*C* predicts that reaction of peroxo-$Fe_2^{III/III}$-AurF with limiting Ar-NH_2 in the absence of excess O_2 should generate equal quantities of two distinct diiron products (highlighted in boxes). The first oxidation should produce Ar-NHOH and μ-oxo-$Fe_2^{III/III}$-AurF. The Ar-NHOH so produced should then dissociate from μ-oxo-$Fe_2^{III/III}$-AurF and react with a second equivalent of peroxo-$Fe_2^{III/III}$-AurF to generate Ar-NO_2 and $Fe_2^{II/II}$-AurF. In our previous study (11), O_2 was present in excess, which (we now understand) must have converted the $Fe_2^{II/II}$-AurF (the reduced product of the Ar-NHOH → Ar-NO_2 oxidation) back to peroxo-$Fe_2^{III/III}$-AurF (red arrows), thereby preventing detection of the reduced enzyme form. We therefore tested the prediction of Scheme 1*C* by Mössbauer spectroscopy on samples prepared with limiting O_2. A sample was enriched in peroxo-$Fe_2^{III/III}$-AurF by reaction of $Fe_2^{II/II}$-AurF with 0.75 equiv O_2. The Mössbauer spectrum of this sample (Fig. 2*K*, vertical bars) confirms that peroxo-$Fe_2^{III/III}$-AurF is the major species (72%, red line). The spectrum of an identical sample that was subsequently treated with 0.19 equiv Ar-NH_2 and allowed to react to completion (4 s) prior to being freeze-quenched shows marked differences (Fig. 2*L*). Analysis of the *L*-*K* difference spectrum (Fig. 2*M*, vertical bars) indicates that 29% of peroxo-$Fe_2^{III/III}$-AurF (red line) is converted to 17% μ-oxo-$Fe_2^{III/III}$-AurF (green line) and 12% $Fe_2^{II/II}$-AurF (blue line). The sum of these spectral contributions (Fig. 2*M*, black solid line) reproduces the experimental difference spectrum well. The total loss of intensity attributable to peroxo-$Fe_2^{III/III}$-AurF is only 76% of the theoretical value: 0.19 equiv Ar-NH_2 should consume 0.38 equiv peroxo-$Fe_2^{III/III}$-AurF complex, resulting in a loss of 38% (compared to the observed 29%) of total intensity. The yield of μ-oxo-$Fe_2^{III/III}$ – AurF is within experimental error of the theoretical value (17% compared to 19%), but the yield of $Fe_2^{II/II}$-AurF is only ∼60% of the theoretical value (12% compared to 19%). As argued above, the observed yield of $Fe_2^{II/II}$-AurF and observed consumption of peroxo-$Fe_2^{III/III}$-AurF are

most likely diminished from their theoretical values by exposure to atmospheric O_2 in the freeze-quench procedure, which results in conversion of a fraction of the $Fe_2^{II/II}$-AurF product (~7% of the total absorption intensity, essentially the same as in Fig. 2*C*) back to peroxo-$Fe_2^{III/III}$-AurF. The important point is that both products predicted by Scheme 1*C* are readily detected.

Discussion

AurF catalyzes the six-electron oxidation of Ar-NH_2 to Ar-NO_2 (2). All previous studies assumed that this conversion entails three sequential two-electron oxidations (Scheme 1*A*) (8–10). Of the two proposed intermediates in this sequence, Ar-NHOH and Ar-NO, the former compound was unequivocally identified (6) and reasonably presumed to form in the rapid reaction of peroxo-$Fe_2^{III/III}$-AurF with Ar-NH_2 (11). In this study, we investigated the reaction of this first intermediate, Ar-NHOH, with peroxo-$Fe_2^{III/III}$-AurF. Surprisingly, this reaction couples the oxidation of Ar-NHOH by four electrons (to Ar-NO_2) to the complete reduction of peroxo-$Fe_2^{III/III}$-AurF to $Fe_2^{II/II}$-AurF (Scheme 1*B*). The proposed intermediates in this reaction, Ar-NO or Ar-N$(OH)_2$ and a $Fe_2^{III/III}$ cluster, apparently do not accumulate substantially during the reaction (even in the active site during a single turnover), as implied by the near identity of the Mössbauer difference spectra at different reaction times (Fig. 2, spectra *D*, *E*, *I*, and *J*) and the ability to account for these spectral changes by summation of the spectra of only the reactant and product states (peroxo-$Fe_2^{III/III}$-AurF and $Fe_2^{II/II}$-AurF).

This finding can explain several published observations and has implications for the mechanism of the Ar-NHOH → Ar-NO_2 conversion by AurF. The reaction entails, formally, transfer of an O-atom from the peroxide moiety of peroxo-$Fe_2^{III/III}$-AurF to Ar-NHOH and transfer of two H-atoms from Ar-NHOH to the diiron cluster. The Hertweck group proposed that this conversion might proceed by a sequence of hydroxylation of Ar-NHOH to Ar-N$(OH)_2$, elimination of water to form Ar-NO, and transfer of a second O-atom to yield Ar-NO_2 (Scheme S1, right branch) (7, 8). They attempted to identify the proposed Ar-NO intermediate but failed to do so, despite employing a sensitive assay. They concluded that "rapid and possibly spontaneous turnover" of this intermediate to Ar-NO_2 could rationalize their failure to detect it (7). Their result is consistent with our observation that the presumptive intermediates in the four-electron conversion of Ar-NHOH to Ar-NO_2 do not accumulate.

The Zhao group proposed a different mechanism, founded on the presumption that Ar-NO is an obligatory intermediate on the pathway to Ar-NO_2 (Scheme 1*A*) and the observation that oxidation of Ar-NHOH in the presence of $^{18}O_2$ gas results in production of Ar-NO_2 with at most one atom of ^{18}O (6, 10). As explained by Scheme S1, the authors interpreted this result to imply that the oxidation of Ar-NHOH to Ar-NO must be a direct dehydrogenation, rather than the hydroxylation-dehydration sequence proposed by Hertweck. The presumed intermediacy of Ar-NO also understandably led the Zhao group to search for this intermediate, which they purported to identify by HPLC with initial UV absorption detection followed by mass spectrometric (MS) detection of a fragment ion of appropriate mass-to-charge ratio (m/z) to be the decarboxylation product of the Ar-NO molecular ion (10). We suggest that the Ar-NO detected by Zhao and coworkers could have arisen from nonenzymatic oxidation or disproportionation of Ar-NHOH (a true accumulating intermediate in the AurF sequence) rather than as a product of the AurF reaction. Supporting this view, we have repeatedly detected by HPLC-MS measurements on solutions of Ar-NHOH dissolved in O_2-containing buffer (with or without AurF) a species of the correct m/z to be the Ar-NO parent ion (Fig. S4). Our inference is also corroborated by the Hertweck group's detection of the dimerized substrate species, azoxybenzol-4,4′-dicarboxylic acid, which, they proposed, could have formed nonenzymatically via an Ar-NO intermediate (7).

Whereas it is possible that the substrate, Ar-NH_2 (Ar-NHOH), could either rapidly trap a more reactive (e.g., $Fe_2^{IV/IV}$) complex with which peroxo-$Fe_2^{III/III}$-AurF rapidly interconverts or, upon binding, could trigger the rapid conversion of the peroxide intermediate to the *N*-oxygenating complex, we presume for the purposes of this discussion that the peroxide complex is itself the *N*-oxygenating species. The hydroxylation of Ar-NH_2 is likely to involve nucleophilic attack of the amine on the peroxide moiety of peroxo-$Fe_2^{III/III}$-AurF (11). Hydroxylation of Ar-NHOH could also proceed by nucleophilic attack of the N-atom on the peroxide O-atom. Indeed, Ar-NHOH is expected to be even more nucleophilic than Ar-NH_2 as a result of the so-called alpha effect (13). Examination of the published structure of the μ-oxo-$Fe_2^{III/III}$-AurF • Ar-NO_2 complex (10) suggests a relatively simple trajectory for this hydroxylation mechanism (Scheme 2). The peroxide ligand is depicted in a μ-1,1 or distorted μ-η^2:η^2 coordination mode, because the spectroscopic properties of peroxo-$Fe_2^{III/III}$-AurF are different from those of well-characterized μ-1,2-peroxo-$Fe_2^{III/III}$ complexes (14, 15). However, the peroxide moiety could also be protonated (i.e., in a μ-1, 1-hydroperoxo-$Fe_2^{III/III}$ complex), as we previously proposed (11). Nucleophilic attack of the bound Ar-NHOH on the uncoordinated or more distally coordinated O-atom of the (hydro)peroxide moiety would cleave the peroxide O-O bond and transfer an O-atom to the substrate. The product would be the Ar-N$(OH)_2$ intermediate proposed by the Hertweck group, or perhaps its deprotonated form, bound to the resulting $Fe_2^{III/III}$-AurF form. Transfer of two electrons and two protons from Ar-N$(OH)_2$ to the $Fe_2^{III/III}$ cluster (formally, a dehydrogenation), rather than the sequence of dehydration followed by O-atom transfer proposed by the Hertweck group, could then give Ar-NO_2 directly, with the ^{18}O-isotope labeling pattern observed by Zhao and coworkers (Scheme 2 and Scheme S1, middle). The new proposal appears to accommodate all available experimental data. The latter steps might conceivably occur by deprotonation of the Ar-N$(OH)_2$ intermediate, perhaps by the μ-oxo bridge (as depicted in Scheme 2) or one of the protein carboxylate residues (16), followed by inner-sphere electron transfer steps.

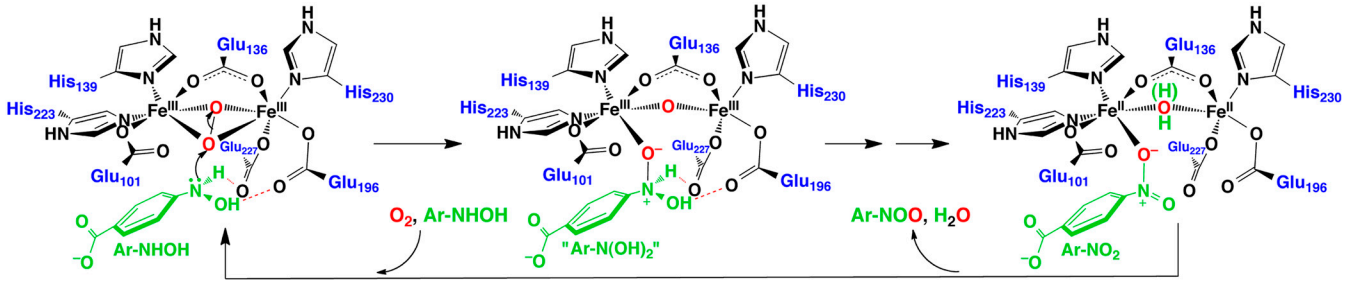

Scheme 2. Proposed mechanism of the four-electron oxidation of Ar-NHOH to Ar-NO_2 by peroxo-$Fe_2^{III/III}$-AurF. The scheme is derived from the X-ray crystal structure of the μ-oxo-$Fe_2^{III/III}$-AurF • Ar-NO_2 complex, Protein Data Bank identification code 3CHT (10).

By contrast, the first step of the Zhao pathway (6, 10), dehydrogenation of Ar-NHOH, is distinct from the aforementioned nucleophilic attack of the substrate on the electrophilic peroxo-$Fe_2^{III/III}$ complex. Distinct reactivities of intermediates with similar structures are well documented for the mononuclear non-heme-iron enzymes, in which the Fe^{IV}-oxo (ferryl) unit can act either as electrophile (17), transferring its O-atom to an electron-rich substrate, or as hydrogen-atom-abstractor, initiating hydroxylation, halogenation, desaturation, and cyclization outcomes (18). One-electron oxidation of Ar-NHOH by peroxo-$Fe_2^{III/III}$-AurF with deprotonation and coordination of the resulting aminoxyl radical (Ar-NHO$^{\bullet}$) to the Fe_2 cluster, which is formally an H-atom abstraction akin to those effected by the ferryl intermediates, seems a conceivable reaction pathway on the basis of precedent from inorganic chemistry (19, 20). We anticipate that this step would cleave the O-O bond and generate a high-valent (hydr)oxo-bridged $Fe_2^{III/IV}$-cluster, given that the related peroxo-$Fe_2^{III/III}$ intermediate in the I100W variant of toluene/*o*-xylene monooxygenase converts to a $Fe_2^{III/IV}$ complex upon transfer of an electron from the introduced tryptophan residue (21). Several decay pathways for the hypothetical (hydr)oxo-$Fe_2^{III/IV}$-AurF:Ar-NHO$^{\bullet}$ complex can be envisaged. Transfer of another proton [presumably to one of the bridging oxygenic ligands or a protein carboxylate residue (16)] and another electron via an inner-sphere mechanism would yield formally Ar-NO and a $Fe_2^{III/III}$ cluster. In the final step, this $Fe_2^{III/III}$ cluster would have to serve as an O-atom donor to generate $Fe_2^{II/II}$-AurF and Ar-NO_2. Alternatively, the order of these steps (electron transfer, proton transfer, and O-atom transfer) within the (hydr)oxo-$Fe_2^{III/IV}$-AurF:Ar-NHO$^{\bullet}$ complex could be different.

Of the two general pathways described above, nucleophilic attack of Ar-NHOH on the peroxide moiety versus formal H-atom transfer from Ar-NHOH to the peroxide, we prefer the former pathway (Scheme 2), because it most simply accounts for the outcome of the reaction, implies more similar reactivities of the Ar-NH_2 substrate and Ar-NHOH intermediate toward peroxo-$Fe_2^{III/III}$-AurF, and accounts for all available data. Additional experiments will be required to distinguish among these and other mechanistic possibilities.

Experimental Procedures

Materials. AurF was prepared as previously described (11). Ar-NHOH was synthesized according to a published procedure (22). Its purification and characterization are detailed in *SI Text* and Figs. S6 and S7.

AurF Turnover Assay. Catalytic conversion of Ar-NHOH to Ar-NO_2 was demonstrated by using RP-HPLC to resolve the two compounds and UV absorption to detect them. Comparison of the chromatograms of assay and control samples to that of a standard mixture of Ar-NH_2, Ar-NHOH, and Ar-NO_2 was used to quantify the Ar-NHOH substrate remaining and Ar-NO_2 product generated (Fig. 3). The standard mixture was prepared by dissolving the solids in 50 mM HEPES buffer (5% glycerol, pH 7.5) to a final concentration of 400 μM of each. The reaction was carried out in the same buffer, which was saturated with O_2 at 0 °C by vigorous stirring on ice under 1.1 atm of the gas. Immediately before initiation of the reaction by addition of enzyme, Ar-NHOH was dissolved in the O_2-saturated buffer to a final concentration of 450 μM. $Fe_2^{II/II}$-AurF (1.0 mM) was prepared by treating as-isolated AurF with one equiv sodium dithionite for 30 min at room temperature in the absence of O_2. After a brief (~30 s) exposure to air the $Fe_2^{II/II}$-AurF was added to the reaction system to a final concentration of 15 μM. The solution was stirred on ice for 20 min and then filtered through an Amicon Ultra-0.5 centrifugal filter (10,000 molecular weight cut-off; Millipore) at 4 °C (13,000 rpm, 10 min). The filtered solution was analyzed by RP-HPLC as described in *SI Text*. An otherwise identical sample lacking only $Fe_2^{II/II}$-AurF served as the control for this reaction.

ACKNOWLEDGMENTS. We thank Tyler L. Grove and Denise A. Conner for assistance in preparation and characterization of the synthetic Ar-NHOH, Gang Xing for assistance in the RP-HPLC analysis, and Megan L. Matthews for preparation of Fig. 3 and Scheme S1 and for advice on Schemes 1 and 2.

1. Hirata Y, Nakata H, Yamada K, Okuhara K, Naito T (1961) Structure of aureothin, a nitro compound obtained from *Streptomyces thioluteus*. *Tetrahedron* 14:252–274.
2. He J, Hertweck C (2004) Biosynthetic origin of the rare nitroaryl moiety of the polyketide antibiotic aureothin: Involvement of an unprecedented *N*-oxygenase. *J Am Chem Soc* 126:3694–3695.
3. Wallar BJ, Lipscomb JD (1996) Dioxygen activation by enzymes containing binuclear non-heme iron clusters. *Chem Rev* 96:2625–2657.
4. Merkx M, et al. (2001) Dioxygen activation and methane hydroxylation by soluble methane monooxygenase: A tale of two irons and three proteins. *Angew Chem Int Edit* 40:2782–2807.
5. Nordlund P, Reichard P (2006) Ribonucleotide reductases. *Annu Rev Biochem* 75:681–706.
6. Simurdiak M, Lee J, Zhao H (2006) A new class of arylamine oxygenases: Evidence that *p*-aminobenzoate *N*-oxygenase (AurF) is a di-iron enzyme and further mechanistic studies. *ChemBioChem* 7:1169–1172.
7. Winkler R, Hertweck C (2005) Sequential enzymatic oxidation of aminoarenes to nitroarenes via hydroxylamines. *Angew Chem Int Edit* 44:4083–4087.
8. Winkler R, et al. (2007) A binuclear manganese cluster that catalyzes radical-mediated *N*-oxygenation. *Angew Chem Int Edit* 46:8605–8608.
9. Krebs C, Matthews ML, Jiang W, Bollinger JM, Jr (2007) AurF from *Streptomyces thioluteus* and a possible new family of manganese/iron oxygenases. *Biochemistry* 46:10413–10418.
10. Choi YS, Zhang H, Brunzelle JS, Nair SK, Zhao H (2008) *In vitro* reconstitution and crystal structure of *p*-aminobenzoate *N*-oxygenase (AurF) involved in aureothin biosynthesis. *Proc Natl Acad Sci USA* 105:6858–6863.
11. Korboukh VK, Li N, Barr EW, Bollinger JM, Jr, Krebs C (2009) A long-lived, substrate-hydroxylating peroxodiiron(III/III) intermediate in the amine oxygenase, AurF, from *Streptomyces thioluteus*. *J Am Chem Soc* 131:13608–13609.
12. Broadwater JA, Achim C, Münck E, Fox BG (1999) Mössbauer studies of the formation and reactivity of a quasi-stable peroxo intermediate of stearoyl-acyl carrier protein Δ^9-desaturase. *Biochemistry* 38:12197–12204.
13. Buncel E, Um I-H (2004) The α-effect and its modulation by solvent. *Tetrahedron* 60:7801–7825.
14. Kim K, Lippard SJ (1996) Structure and Mössbauer spectrum of a (μ-1,2-peroxo)bis(μ-carboxylato)diiron(III) model for the peroxo intermediate in the MMO hydroxylase reaction cycle. *J Am Chem Soc* 118:4914–4915.
15. Skulan AJ, et al. (2004) Nature of the peroxo intermediate of the W48F/D84E ribonucleotide reductase variant: Implications for O_2 activation by binuclear non-heme iron enzymes. *J Am Chem Soc* 126:8842–8855.
16. Do LH, Hayashi T, Moënne-Loccoz P, Lippard SJ (2010) Carboxylate as the protonation site in (peroxo)diiron(III) model complexes of soluble methane monooxygenase and related diiron proteins. *J Am Chem Soc* 132:1273–1275.
17. Eser BE, et al. (2007) Direct spectroscopic evidence for a high-spin Fe(IV) intermediate in tyrosine hydroxylase. *J Am Chem Soc* 129:11334–11335.
18. Krebs C, Galonić Fujimori D, Walsh CT, Bollinger JM, Jr (2007) Non-heme Fe(IV)-oxo intermediates. *Acc Chem Res* 40:484–492.
19. More KM, Eaton GR, Eaton S (1987) Metal-nitroxyl interactions. 52. EPR spectra of nitroxyl radicals coordinated to manganese(III) tetraphenylporphyrin via the nitroxyl oxygen. *Inorg Chem* 26:2618–2620.
20. Dikalov SI, Vitek MP, Maples KR, Mason RP (1999) Amyloid β peptides do not form peptide-derived free radicals spontaneously, but can enhance metal-catalyzed oxidation of hydroxylamines to nitroxides. *J Biol Chem* 274:9392–9399.
21. Murray LJ, et al. (2007) Dioxygen activation at non-heme diiron centers: Oxidation of a proximal residue in the I100W variant of toluene/o-xylene monooxygenase hydroxylase. *Biochemistry* 46:14795–14809.
22. Bauer H, Rosenthal SM (1944) 4-Hydroxylaminobenzenesulfonamide, its acetyl derivatives and diazotization reaction. *J Am Chem Soc* 66:611–614.